

**DETC2017/67837**

## **DESIGN OF WEARABLE LOWER LEG ORTHOTIC BASED ON SIX-BAR LINKAGE**

**Shramana Ghosh \***

Department of Mechanical  
and Aerospace Engineering  
University of California  
Irvine, California 92697  
Email: shramang@uci.edu

**Nina Robson**

Mechanical Engineering Department  
California State University  
Fullerton, California 92834  
Email: nrobson@exchange.fullerton.edu

**J. M. McCarthy**

Department of Mechanical  
and Aerospace Engineering  
University of California  
Irvine, California 92697  
Email:jmmccart@uci.edu

### **ABSTRACT**

*The paper presents the design of a lower leg orthotic device based on dimensional synthesis of multi-loop six-bar linkages. The wearable device is comprised of a 2R serial chain, termed the backbone, sized according to the wearer's limb anthropometric dimensions. The paper is a result of our current efforts in proposing a systematic process for the development of 3D printed customized assistive devices for patients with reduced limb mobility, based on anthropometric data and physiological task.*

*To design the wearable device, the physiological task of the limb is obtained using an optical motion capture system and its dimensions are set such that it matched the lower leg kinematics as closely as possible. As a next step a six-bar linkage is synthesized and ensured that its motion is as close as possible to the physiological task. Next, the 2R backbone is replaced by the wearer's limb to provide the skeletal structure for the multi-loop wearable device. During the final stage of the process the 2R backbone is relocated to parallel the human's limb on one side, providing support and stability. The designed device can be secured to the thigh of the user to guide the lower leg without causing any discomfort and to ensure a natural physiological gait trajectory. This results in orthotic device for assisting people with lower leg injuries with compact size and better wearability.*

### **INTRODUCTION**

Understanding and exploiting the biomechanics of human walking is crucial for the design of any orthotic device for the lower limbs. The human leg kinematics can be represented as a seven Degrees of Freedom (DOFs) chain, with three rotational DOFs at the hip and four at the lower leg (one at the knee, and three at the ankle). More detailed anatomical studies, however, show that the human knee joint is a complex structure that displays angular movement in three dimensions and translation in one dimension relative to the hip during walking. However, compared to the most significant angular motion, flexion-extension in the sagittal plane, the amplitudes of the other movements are relatively small [1]. Similarly the motion of the ankle joint is characterized by plantarflexion - dorsiflexion. Thus in the sagittal plane, which is the dominant plane of motion during walking, the structure of the lower leg can be simplified to a 2R chain as shown in Figure 1, with revolute joints at the knee and the ankle. This simplified kinematic structure is at the heart of the kinematic design of many exoskeleton or orthotic devices to provide the required assistive action.

While the terms orthosis and exoskeleton are sometimes used interchangeably, Dollar and Herr [2] classify an orthosis as an anthropomorphic wearable device that is used to increase the ambulatory ability of a person suffering from a leg pathology by working in concert with the operator's movements. Exoskeletons, on the other hand, are defined as devices that augment the performance of an able-bodied wearer. One of the earliest orthotic devices that used a simple mechanism to simulate walking

---

\* Address all correspondence to this author.

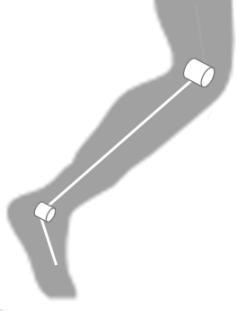


**FIGURE 1.** The kinematic structure of the lower leg in the sagittal plane.

was patented by Cobb [3]. It consisted of a leg brace with a crank located at the hip that was used to wind up a torsional spring located at the knee joint, and produced a reciprocating motion at the knee via a cam and follower. Another early example of a design that reduced the difficulties encountered in the control of a large number of servo systems to obtain a certain gait trajectory by using kinematic coupling between the hip and the knee can be seen in the "kinematic walker" [4].

Exploiting the dynamics of human walking and the leg morphology via the use of kinematic programming allows us to create lighter and more efficient devices. Other orthotic devices that use kinematic programming include the Powered Gait Orthosis (PGO), which is a one DOF system for each leg having a mechanized hip and knee design, along with a cam - modulated linkage for knee function generation with variable time ratio [5]. A combination of springs and linkages are used by the passive leg orthosis developed at University of Delaware in order to geometrically locate the center of mass of the leg - orthosis system, and then, balance out the effect of gravity [6]. A comprehensive study of lower-limb exoskeleton and orthotic designs can be found in [2].

Some of the major concerns related to the mechanical design of the orthotics include the problems associated with closely matching and obtaining close alignment between the structure of the exoskeleton to the wearer, portability, and the affectation of the biomechanics of locomotion due to added mass and inertia of the device itself as well as the additional kinematic constraints inadvertently imposed on the wearer. Some commonly used techniques for interfacing an orthotic with the lower limb of a wearer include foot connections [4] or specialized shoes [7] and straps, cuffs or harnesses around the thighs [7] and calves [8].

The issue of portability and safety are major factors that limit the application of orthoses outside of clinical therapy. Interestingly most powered orthotic devices still require the use of crutches or another additional support method for the user [2]. However, there is great value in developing portable orthotic devices that can be used during the wearers every day life without

the need for constant medical supervision.

It is important to note that while most of the underactuated parallel or multi-loop exoskeleton devices in literature show satisfactory performance, there still does not exist a systematic methodology for the design of these systems that make use of the human body's anatomical structure. Hence, there is a need for the development of design techniques for passive linkages based on skeletal structures. The paper was inspired by the idea of proposing a systematic process for development of 3D printed customizable limb-assistive devices based on anthropometric limb data and physiological tasks in home settings. In this paper we extend upon the work in Robson and Soh [9] regarding designing eight bar slider exo-hand devices to show that it is possible to create orthotic devices by following similar techniques. The latter includes identifying the desired limb motion by using motion capture system, mathematically describing the limb trajectory as physiological task, linkage topology selection, dimensional synthesis and linkage assessment.

Here, we would like to note that unlike other wearable device design techniques that use parallel mechanical linkages, we offer a novel alternative approach: a comprehensive systematic process to create wearable lower extremity devices that incorporate anthropometric backbone chain and physiological task.

## GENERAL DEVELOPMENT PROCESS

This work is part of our efforts in establishing a systematic process for the development of 3D printed customized upper and lower extremity assistive devices, based on anthropometric limb data and physiological task. The overall process is shown in Figure 2.

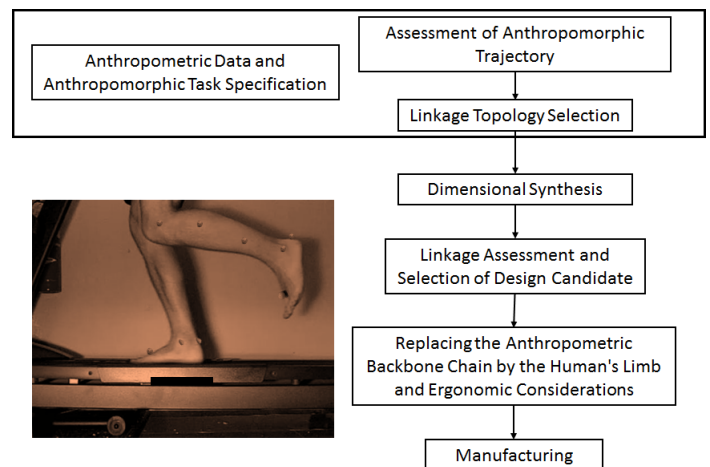


**FIGURE 2.** The systematic process for development of 3D printed customized upper and lower extremity assistive devices.

The customized assistive device is based on anthropomorphic measurements of the user's limb and is built specifically to mimic their natural physiological task performance. This information can be easily collected using various types of motion capture technologies available commercially. Depending on the complexity of the physiological task to be supported, a linkage topology is selected. This selection is dependent on the designer's experience, although with the advent of many commercially available mechanism synthesis packages (e.g. MechGen [10], MotionGen [11]), a number of different linkage topologies can be easily explored. Once the dimensional synthesis process is carried out, task- and limb-specific assessment criteria are employed to identify the most suitable design candidate. This design candidate is then modified and the anthropometric backbone chain is replaced with the biological limb. At the end of the process, additional design adjustments are made to ensure the device is stable and ergonomic. A 3D printed prototype can then be manufactured.

### DEVELOPMENT OF A WEARABLE LOWER LEG SIX-BAR ORTHOTIC

Our goal is to design mechanical six-bar linkage orthotic device, based on anthropometric data from a human lower extremity that can mimic as closely as possible humans' natural walking gait trajectory, as well as can be easily paired with the human limb, avoiding collision between the linkage and the wearer's limb. In Soh [12] the entire human leg has been approximated by a spatial serial TRS chain and dimensional synthesis is used to obtain a two DOF spatial eight-bar linkage to mimic walking. More recently, Plecnik and McCarthy [13] illustrated the design of the lower leg orthotic device based on a Stephenson II six-bar function generators for 11 accuracy points. This work was further extended to present the design of an optimized Stephenson III six-bar linkage for following the natural ankle trajectory by Tsuge et al. [14]. In 2016 Robson and Soh [9] presented the idea of using the human's actual limb to replace the backbone chain of a linkage in the design of wearable devices.

### Anthropometric Data and Assessment of Anthropomorphic Task Trajectory

The design approach starts by obtaining experimental data of a healthy human subject walking on a treadmill at a speed of 1.2 m/s. Normal walking speed for healthy adults is reported to be  $1.4 \pm 0.2$  m/s [15]. A loss of motion and slower walking speed is commonly seen in patients with neurological gait deficits, and at lower walking speeds it has been found that the hip and the knee demonstrate decreased flexion during swing phase in the sagittal plane [16]. For clinical gait rehabilitation training, encouraging normal to faster than normal walking speeds may be advantageous, as proposed by Behrman and Harkema [17] and

Sullivan et al. [18]. Keeping this in mind, we obtain the target kinematics at a self-selected normal walking speed for the subject. The kinematics of the motion are obtained by attaching infrared markers to the lower body of the subject (as illustrated in Figure 3 (a)). The recorded data conveys frame-by-frame information about the positions of the rigid segments of the lower body, namely the trunk, thighs, shank and feet, as shown in Figure 3 (b).

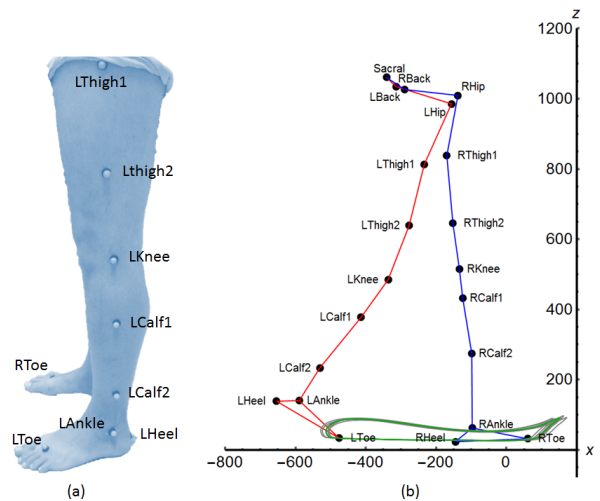


**FIGURE 3.** (a) Marker placement on the lower leg of the healthy subject. (b) Motion capture still of the lower body along with the captured trajectories (gray) and the averaged trajectory (green) of the Left Toe marker.

In the sagittal plane, the trajectory traced by the foot resembles the well known 'teardrop' shape, shown in Figure 3 (b). The gait data obtained may vary across different trials, yet the qualitative nature of the data remains similar. The human walking cycle is typically represented as starting and ending at heel strike on the same foot, as shown in Figure 4. The stance phase, which involves the foot under observation being in contact with the ground takes up 60% of the gait cycle (heel strike to toe off), and is followed by the swing phase. This average trajectory of the Left Toe marker displayed in Figure 3 (b) in green is given with respect to a global fixed frame set on the ground. However, in order to look at the motion of the lower leg in isolation, the thigh is held stationary. Figure 5 shows the positions of the infrared markers attached to the body transformed relative to a new fixed frame attached to the thigh, as well as the new trajectory traced by the foot relative to the thigh fixed frame.

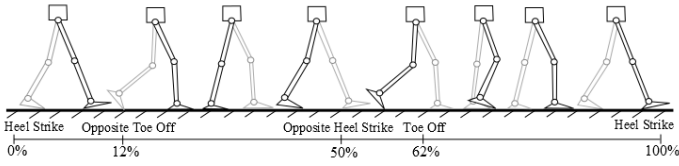


**FIGURE 4.** Human walking gait through one cycle in the sagittal plane, beginning and ending at heel strike (adapted from [2]).

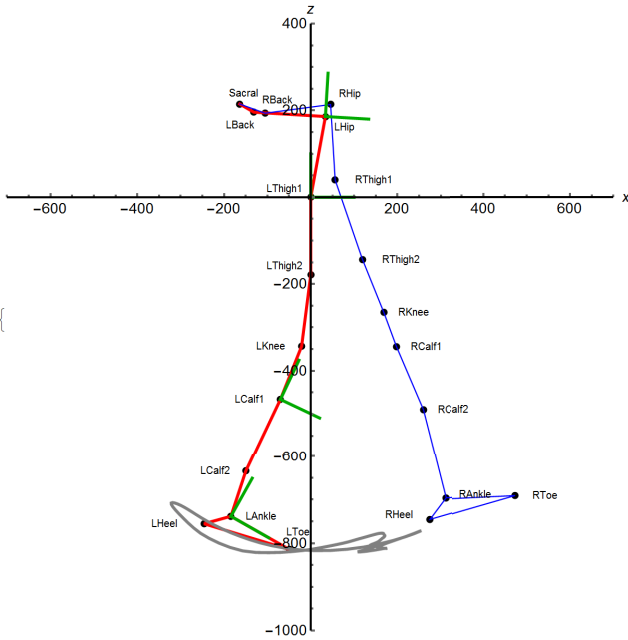


**FIGURE 5.** Trajectory traced by the toe point in the sagittal plane when the thigh is held stationary.

### Linkage Topology Selection

Orthotic devices with complex biomimetic motion can be programmed more successfully using six-bar linkages as compared to four-bar mechanisms as they have more design parameters and hence can coordinate more accuracy points for a given trajectory. In addition, six-bar linkages allow for the choice of the fixed pivot locations, which is an important criteria in the design of wearable devices, as detailed in the *Candidate Assessment* subsection. The synthesis formulation and solution of generic six-bar function generators is described in depth in Plecnik and McCarthy [13]. Function generation refers to the type of kinematic synthesis in which the dimensions of linkages are found that can coordinate the angles of the input and output links in a specified fashion. In addition, Plecnik and McCarthy show that the ability to mechanically program the joint angles of a serial chain can imitate biological movement with one DOF [19].

It can be seen from Figure 4 that in the sagittal plane, the

human lower leg can be approximated by using a 2R serial chain. Thus, we utilize Plecnik and McCarthy’s [19] method to design a six-bar linkage that has a 2R serial chain as the backbone in order to co-locate the knee and the ankle joints of the device with the human operator’s joints. The dimensions of the 2R chain are selected in order to approximate the kinematics of the right lower leg of a subject as closely as possible, i.e. according to Figure 6 the fixed pivot **B** of the RR chain is placed at the right knee, and the moving pivot **F** is located at the right ankle. The link lengths  $l_1$  and  $l_2$  correspond to the average lengths of the right shank (from knee to ankle) and the foot (from ankle to end of the fore foot) are shown in Figure 6 and detailed in Table 1.

<b>B</b> (mm)	<b>F</b> (mm)	$l_1$ (mm)	$l_2$ (mm)
(0, -370)	(-180.56, -732.53)	405	155

**TABLE 1.** Selected dimensions for the 2R backbone chain of the walking device.

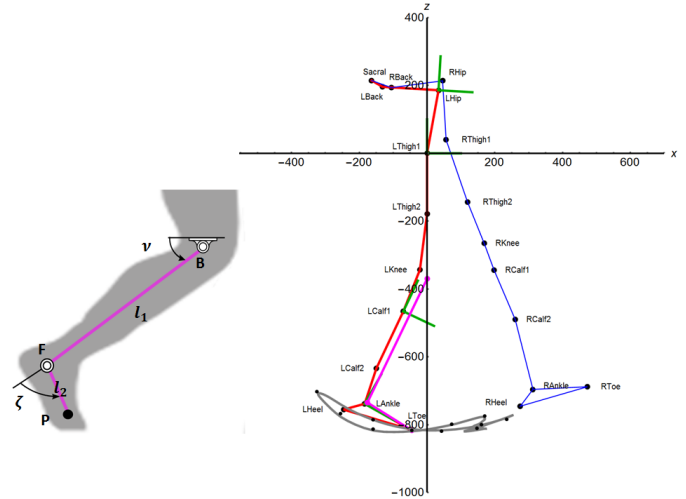


**FIGURE 6.** 2R backbone chain representing the lower leg in the sagittal plane.

The next step in the process is to synthesize a Stephenson II six-bar function generator that incorporates the already specified backbone chain to yield smooth movement throughout the desired task. The resulting linkage design is a scaled kinematic inversion of the function generator as shown by Plecnik and McCarthy [20]. The Stephenson II function generator yields a Stephenson III path generator with the trace point **P** on the ternary link **FHP** as shown in Figure 7. The selection of the

11 positions for the 2R chain based on the kinematics of natural walking are detailed in Figure 8. The eleven configurations of the 2R chain defined by points  $\mathbf{P}_j, j = 0, \dots, 10$ , along the target walking trajectory provide a set of coordinated joint angles ( $v$  and  $\zeta$ ) that are converted to  $\psi$  and  $\phi$  and used as the accuracy points for the design of the Stephenson II function generators. These sets of angles obtained for 11 task positions of the 2R chain shown in Figure 9 and detailed in Table 2.

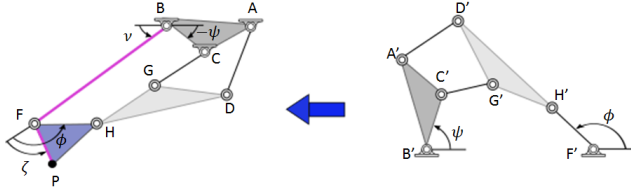


**FIGURE 7.** A Stephenson III path generator obtained by coordinating the RR joints with a Stephenson II function generator (adapted from [20]).

Task Pos. #	$\mathbf{P}$ (mm)	$v$ (rad)	$\zeta$ (rad)	$\psi$ (rad)	$\phi$ (rad)
1	(-49.03, -814.55)	-2.03	1.48	0.00	0.00
2	(-162.88, -809.67)	-2.25	1.31	0.22	-0.16
3	(-256.86, -763.49)	-2.47	1.31	0.44	-0.17
4	(-326.33, -697.47)	-2.69	1.36	0.66	-0.11
5	(-163.13, -781.99)	-2.30	1.50	0.27	0.03
6	(38.50, -816.88)	-1.84	1.47	-0.19	-0.01
7	(141.99, -808.93)	-1.59	1.37	-0.44	-0.10
8	(229.62, -783.63)	-1.38	1.28	-0.65	-0.19
9	(155.56, -799.66)	-1.56	1.40	-0.47	-0.07
10	(165.21, -774.79)	-1.55	1.55	-0.49	0.07
11	(67.46, -797.2)	-1.78	1.58	-0.25	0.10

**TABLE 2.** Coordinates of point  $\mathbf{P}$  on the 2R backbone chain at the task positions selected for synthesis task, and the corresponding values of  $v$  and  $\zeta$ , the input and output of the 2R serial chain and,  $\psi$  and  $\phi$ , the input and output angles of the Stephenson II function generator. .

## Dimensional Synthesis: Stephenson II Function Generation

In this subsection we briefly discuss the synthesis of a Stephenson II six-bar function generator for 11 accuracy points as shown by Plecnik and McCarthy [13].

A Stephenson II linkage is shown in Figure 10. The coordinates of the seven revolute joints of the linkage are defined by complex vectors  $\mathbf{A}, \mathbf{B}, \mathbf{C}, \mathbf{D}, \mathbf{E}, \mathbf{G}$  and  $\mathbf{H}$ . Angles  $\phi, \rho, \psi, \theta$  and  $\mu$  are measured from the reference position to the configuration of the linkage at the  $j^{\text{th}}$  accuracy point, where  $j = 0, \dots, 10$ . The synthesis objective is to find pivot locations to coordinate input angles  $\psi$  and output angles  $\phi$  at the 11 accuracy points selected by the user (enumerated in Table 2).

The ground pivots  $\mathbf{B}$  and  $\mathbf{F}$  become the first link of the 2R backbone chain as shown in Figure 7, hence their position is specified by the designer based on experimental data. Pivot positions  $\mathbf{A}, \mathbf{C}, \mathbf{D}, \mathbf{G}$  and  $\mathbf{H}$  are parameters to be determined by the synthesis process.

In the  $j^{\text{th}}$  configuration, four loop equations can be written to define the linkage, as shown below:

$$\begin{aligned}
 C_j &= B + S_j(C - B) \\
 A_j &= B + S_j(A - B) \\
 G_j &= F + Q_j(H - F) + R_j(G - H) \\
 D_j &= F + Q_j(H - F) + R_j(D - H) \quad j = 1, \dots, 10 \quad (1)
 \end{aligned}$$

And the complex rotation operators can be defined as:

$$\begin{aligned}
 Q_j &= e^{i\Delta\theta_j} & S_j &= e^{i\Delta\psi_j} \\
 R_j &= e^{i\Delta\rho_j} & T_j &= e^{i\Delta\theta_j} \\
 U_j &= e^{i\Delta\mu_j} & & j = 1, \dots, 10 \quad (2)
 \end{aligned}$$

Then the synthesis equations for the Stephenson II six bar linkage are given by the following complex loop equations:

$$\begin{aligned}
 L_j : T_j(G - C) &= [F + Q_j(H - F) + R_j(G - H)] - [B + S_j(C - B)] \\
 M_j : U_j(D - A) &= [F + Q_j(H - F) + R_j(D - H)] - [B + S_j(A - B)] \\
 & j = 1, \dots, 10 \quad (3)
 \end{aligned}$$

And the associated complex conjugate loop equations are:

$$\begin{aligned}
 \bar{L}_j : \bar{T}_j(\bar{G} - \bar{C}) &= [\bar{F} + \bar{Q}_j(\bar{H} - \bar{F}) + \bar{R}_j(\bar{G} - \bar{H})] - [\bar{B} + \bar{S}_j(\bar{C} - \bar{B})] \\
 \bar{M}_j : \bar{U}_j(\bar{D} - \bar{A}) &= [\bar{F} + \bar{Q}_j(\bar{H} - \bar{F}) + \bar{R}_j(\bar{D} - \bar{H})] - [\bar{B} + \bar{S}_j(\bar{A} - \bar{B})] \\
 & j = 1, \dots, 10 \quad (4)
 \end{aligned}$$

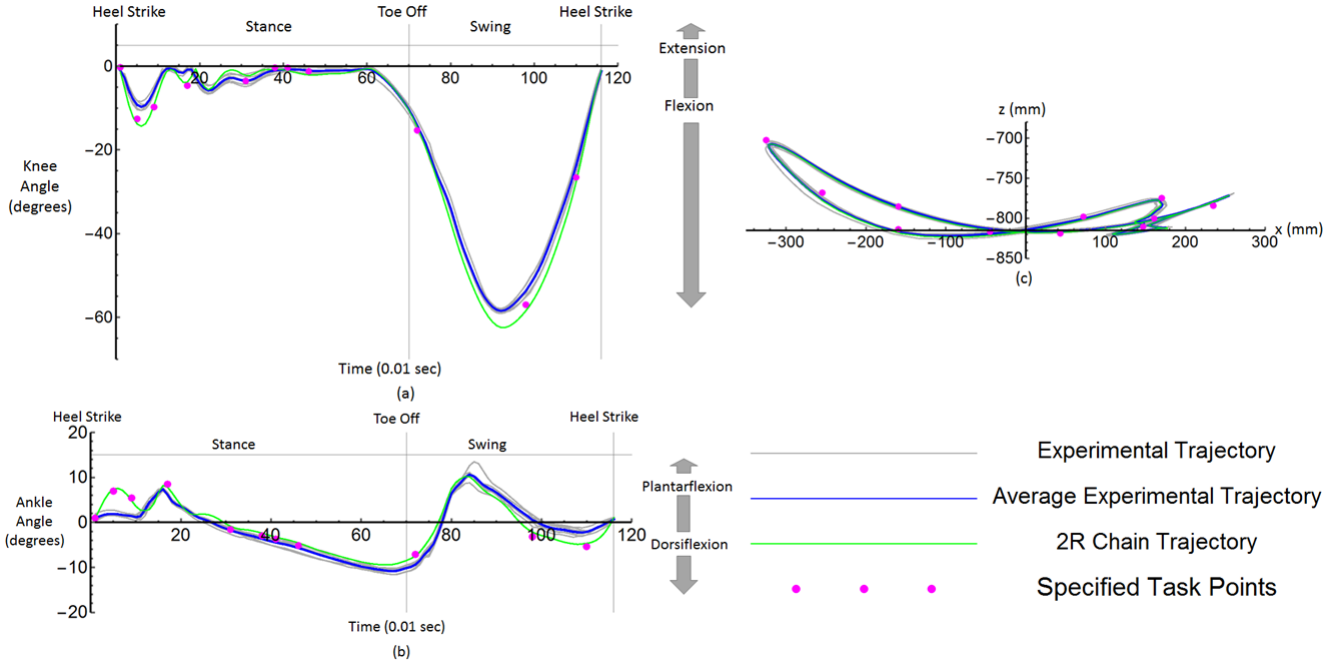


**FIGURE 8.** 2R backbone chain representing the lower leg in the sagittal plane.

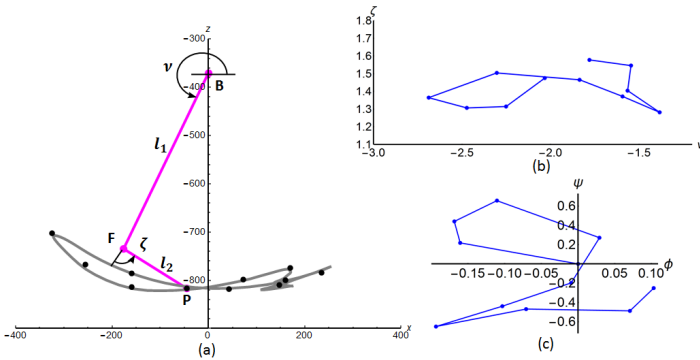


**FIGURE 9.** (a) The 2R chain moving through the 11 specified task positions, (b) The function between  $v$  and  $\zeta$ , the input and output of the 2R serial chain (c) The function between  $\psi$  and  $\zeta$ , the input and output angles of the Stephenson II function generator.

As well as the normalization conditions for complex operators:

$$\begin{aligned} R_j \bar{R}_j &= 1 \\ U_j \bar{U}_j &= 1 \\ T_j \bar{T}_j &= 1 \quad j = 1, \dots, 10 \end{aligned} \quad (5)$$

From equations (3, 4, 5), we can see that for 11 accuracy points represented by configurations  $j = 0, \dots, 10$ , we get 70 equations in 70 unknowns. Plecnick and McCarthy [13] present a method

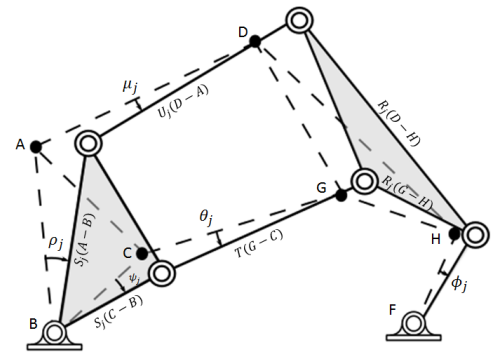


**FIGURE 10.** Stephenson II six bar linkage (adapted from [21]).

to reduce this set of 70 equations in 70 unknowns to a set of equations of degree 8 in 10 design parameters formed by  $\mathbf{A}, \mathbf{C}, \mathbf{D}, \mathbf{G}, \mathbf{H}$  and  $\bar{\mathbf{A}}, \bar{\mathbf{C}}, \bar{\mathbf{D}}, \bar{\mathbf{G}}, \bar{\mathbf{H}}$ . The total degree of the polynomial system is  $8^{10} = 1.07 \times 10^9$ . The generic synthesis equations are solved by Plecnick and McCarthy [13] using regeneration homotopy method with the software package BERTINI. The nonsingular solutions found are used to construct parameter homotopies for efficient calculation of linkage solutions for a specific set of 11 coordinated joint angles.

The time required to solve the synthesis equations is 2 hours, 14 minutes and 21 seconds on a node using UC Irvine high performance computing cluster. Parallel processing was used with

64 CPUs at a speed of 2.2 GHz for each core. We obtain 332 design candidates.

### Linkage Assessment and Selection of Design Candidate

Of the 332 linkage designs obtained, none satisfy all the 11 task points. However, nine of the solutions passed through 10 of the 11 specified points. The task point that is missed is number eight, which results in a reduction of the knee extension by 2.2°, or 3% of the 60° range of motion. Only six linkages (five going through ten positions, and one going through nine positions) are found to be free of order defect, i.e. they go through the specified task positions in the order specified. The pivot locations of these six solutions are presented in Table 3 and the linkage structures are shown in Figure 11.

#	A		B		C	
1	(-35.05, -361.37)		(0, -370)		(55.98, -345.67)	
	D	F	G	H		
	(3.54, -342.59)	(-180.56, -732.53)	(-91.63, -368.68)	(-67.99, -700.67)		
2	(-35.05, -361.37)		(0, -370)		(57.86, -717.25)	
	D	F	G	H		
	(-106.57, -719.459)	(-180.56, -732.53)	(-19.67, -866.22)	(-67.99, -700.67)		
3	(108.8, -235.38)		(0, -370)		(-38.95, -347.93)	
	D	F	G	H		
	(57.5, -219.78)	(-180.56, -732.53)	(-90.91, -327.86)	(21.4, -550.68)		
4	(79.51, -57.85)		(0, -370)		(-38.95, -347.93)	
	D	F	G	H		
	(111.71, -505.47)	(-180.56, -732.53)	(73.37, -570.75)	(21.4, -550.68)		
5	(-33.11, -344.42)		(0, -370)		(71.5, -323.96)	
	D	F	G	H		
	(8.56, -321.57)	(-180.56, -732.53)	(111.24, -347.77)	(-57.84, -708.15)		
6	(78.35, -564.92)		(0, -370)		(-24.94, -406.09)	
	D	F	G	H		
	(107.93, -497.94)	(-180.56, -732.53)	(71.85, -565.28)	(22.13, -547.96)		

**TABLE 3.** Fixed (B, F) and moving (A, C, D, G, H) pivot locations of the 6 defect free linkage solutions obtained from the design process.

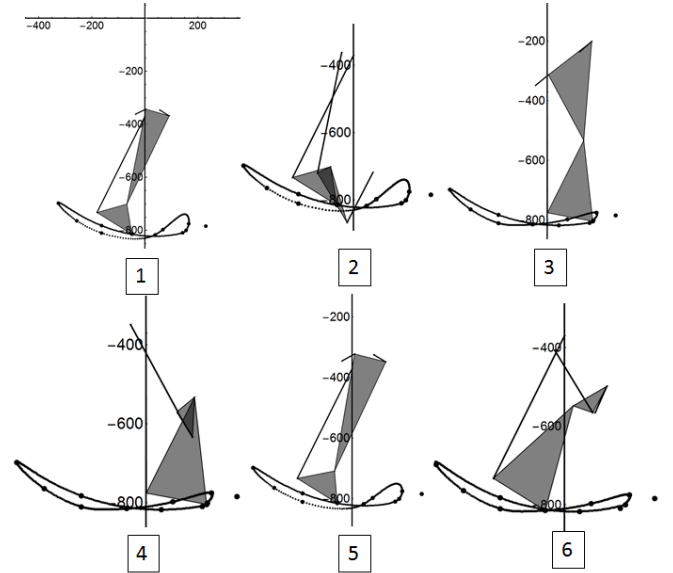


**FIGURE 11.** The four design candidates free of order defect.

The design candidate for the development of the lower leg orthotic should be the linkage which not only goes smoothly through the specified task positions in the specified order, but also interfaces well with the limb of the user and does not impede its natural movement. To eliminate linkages that are unsuitable to being developed into orthotic devices, we identify areas around the lower leg where it is unsuitable to locate the linkage or parts of it (see Figure 12). The area shaded with red locates the area below the second link of the 2R serial chain that mimics the foot, and the presence of any component of the linkage in this region is undesirable as it will cause collisions with the ground and impede natural walking motion. The yellow shaded region identifies the area behind the calf. The presence of the mechanism in this region could increase the chances of collision with the upper leg segment during flexion of the knee affect the gait and cause injuries to the user. Linkage solution two is eliminated from the list of suitable designs based on this assessment.

Next, the linkage designs are evaluated on the basis of the human leg - design candidate system compactness and ranked according to the following formula:

$$S = r_1 + r_2 + A_1 + A_2 \quad (6)$$

where  $r_1$  is the distance of the first fixed pivot **A** from the fixed knee pivot **B**

$r_2$  is the distance of the second fixed pivot **C** from the fixed knee pivot **B**

$A_1$  is the area of the first ternary link, **DGH**

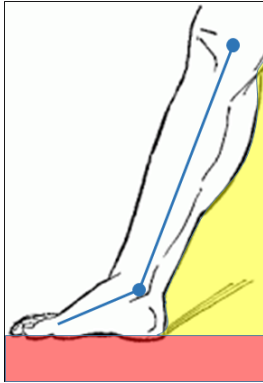


**FIGURE 12.** The regions around the lower leg that determine the suitability of the linkage: the shaded regions are undesirable for locating the linkage.

$A_2$  is the area of the second ternary link, **HFP**.

The most preferred linkage is the one with the lowest  $S$  score and it is found to be linkage solution number one in Figure 11. Figure 13 shows the selected design candidate moving smoothly through the 10 accuracy points.

### Replacing the Anthropometric Backbone Chain by the Humans Limb and Manufacturing

Once the linkage design is selected, we adapt it to the design of a lower leg orthotic device. The 2R anthropometric backbone chain is replaced by the human's lower leg, which becomes the skeletal structure of the orthotic device. To increase balance and stability, the backbone chain 1 of the final design, shown in Figure 14, is relocated to the radial part of the affected leg, collocating the joints with the rotational axes of the human's limb joints to mimic the desired physiological walking trajectory. The chosen design leads to increased safety for the user and a weight balance on both sides of the leg.

During the last stage of the process, many iterations of the design of the first ternary link 2 are considered (see Figure 15), before selecting the final design shown in Figure 14.

The lower part of the second ternary link 3 in Figure 14 approximates the foot of the user. The design of this particular link of the six-bar is additionally enhanced, as shown in Figure 16, in order to securely hold the foot of the wearer.

Another issue is securing the human's leg, which becomes a skeletal part of the linkage itself. While traditionally most devices use Velcro straps to hold the orthotic device in alignment with the supported body, we use double support to ensure safety and stability. A leg-holder 7 in Figure 14 is placed in front of the foot and Velcro straps are used to bind the device with the human limb.

Finally, during the design phase the motion of the foot from

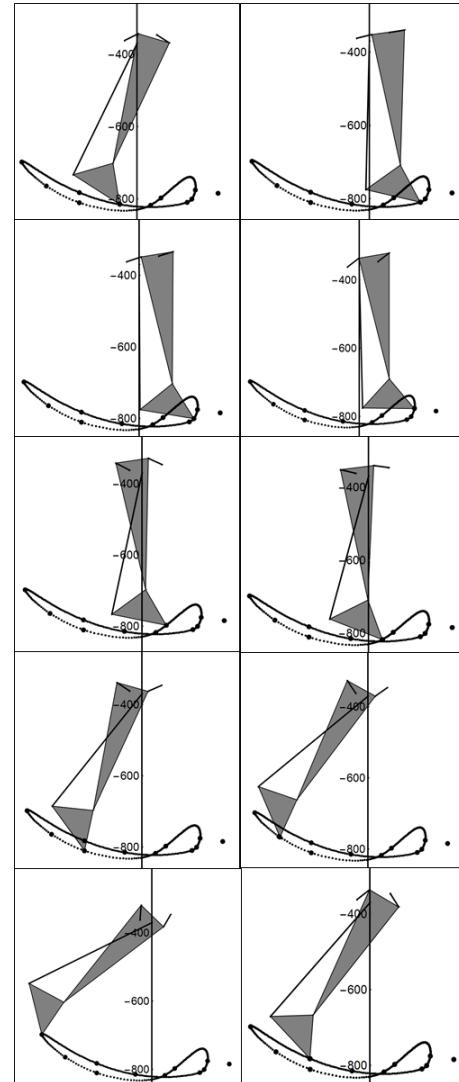


**FIGURE 13.** The selected lower-leg linkage design candidate moving through the 10 specified accuracy points.

the ankle to the 1st metatarsal bone is approximated. The toes cannot be approximated as a rigid body during the walking motion as they flex. In order to allow for this degree of freedom, a passive flexible toe 8 is attached to the foot holder as shown in Figure 14.

A reduced scale of the orthotic device is 3-D printed to test the system and see how all the parts fit together (see Figure 17).

### CONCLUSIONS

The paper describes the design of passive orthotic devices for people with below knee injuries. The device comprises of a 2R serial backbone chain, sized according to the user's anthro-

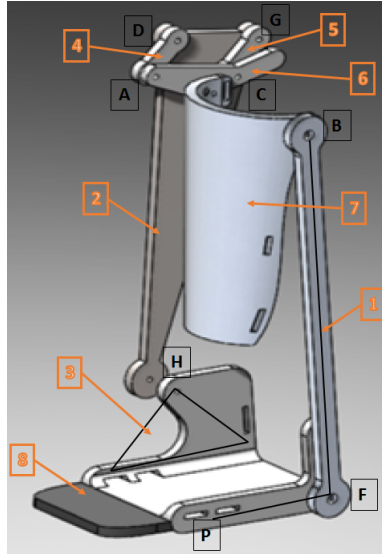


**FIGURE 14.** The design of the lower leg orthotic device adapted from the six-bar linkage selected.

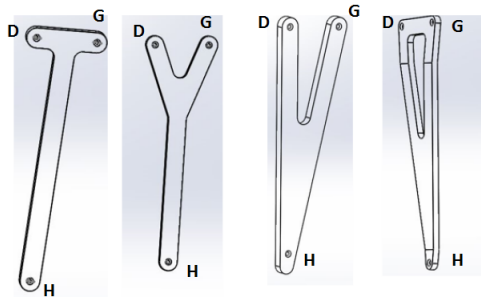


**FIGURE 15.** Different designs for the first ternary link DGH.

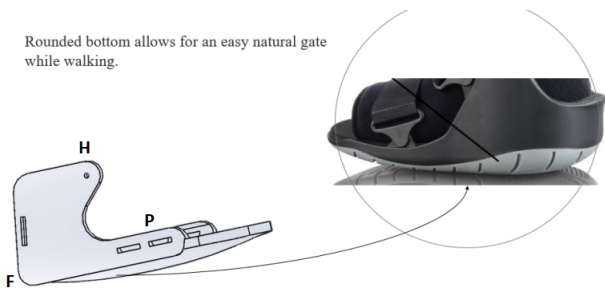


**FIGURE 16.** Adaptation to the second ternary link HFP to transform it into the foot link.

pometric dimensions, which is later constrained to a one DOF six-bar mechanism. We present the design of the wearable device process, starting with physiological task specification, based



**FIGURE 17.** Reduced scale 3D printed model of the orthotic device.

on an optical motion capture data from the movement of the leg and setting the dimensions of the backbone chain to match the lower leg anatomy as closely as possible. To ensure that the six-bar motion is close to the physiological task, a Stephenson II six-bar function generator is synthesized that approximates the motion of the lower leg through 11 task positions. The synthesis equations were solved in 2 hours 14 minutes and 21 seconds on a node using UC Irvine high performance computing cluster. We obtained 332 design candidates, none of which satisfy all the 11 task positions. However, 6 of the solutions are able to pass smoothly through 10 of the specified positions in the correct order. The next step is related to the assessment of these 6 design candidates, based on safety, wearability and compactness and the choice of the most preferred six-bar design. Once the candidate linkage is chosen, the anthropometric 2R backbone chain is substituted with the wearer's limb itself, providing the skeletal structure for the multi-loop wearable device. The 2R backbone is relocated parallel to the human's limb on the radial side, collocating its joints with the human leg rotational axes to provide accurate replication of the natural physiological foot trajectory, as well as to provide better support and stability. This device, having only one degree of freedom can be actuated using either one actuator, or a simple mechanism linking the motion of the thigh to the input of the device. This presents a clear advantage over devices based on a serial architecture as it requires only one actuator to control the entire lower leg.

A reduced scale prototype is 3-D printed to test the system and see how all the parts fit together. Future directions include the development of a full-scale prototype and its performance assessment with respect to ergonomics, safety and stability.

## ACKNOWLEDGMENT

The authors gratefully acknowledge the support of the National Science Foundation (NSF), award Id #1404011. We would like to thank Mark Plecnik, Postdoctoral Scholar at University of California Berkeley for his help in obtaining solutions for 11 point synthesis of Six-bar function generators. We also acknowl-

edge the assistance of Ahmed Shehab, Abdulsahib Al Hazza, Hilan Rocha, Abdullaziz Al Kharas, undergraduate students in Mechanical Engineering department of California State University Fullerton in the development of the 3D prototype.

## REFERENCES

- [1] Lafortune, M., Cavanagh, P. R., Sommer, H., and Kalenak, A., 1992. “Three-dimensional Kinematics of the Human Knee During Walking”. *Journal of biomechanics*, **25**(4), pp. 347–357.
- [2] Dollar, A. M., and Herr, H., 2008. “Lower Extremity Exoskeletons and Active Orthoses: Challenges and State-of-the-art”. *IEEE Transactions on robotics*, **24**(1), pp. 144–158.
- [3] Cobb, G. L., 1935. Walking motion.
- [4] Vukobratovic, M., and Juricic, D., 1969. “Contribution to the Synthesis of Biped Gait”. *IEEE Transactions on Biomedical Engineering*, **BME-16**(1), Jan, pp. 1–6.
- [5] Ruthenberg, B. J., Wasylewski, N. A., and Beard, J. E., 1997. “An experimental device for investigating the force and power requirements of a powered gait orthosis”. *Journal of rehabilitation research and development*, **34**(2), p. 203.
- [6] Banala, S. K., Agrawal, S. K., Fattah, A., Krishnamoorthy, V., Hsu, W.-L., Scholz, J., and Rudolph, K., 2006. “Gravity-balancing leg orthosis and its performance evaluation”. *IEEE Transactions on Robotics*, **22**(6), pp. 1228–1239.
- [7] Walsh, C. J., Pasch, K., and Herr, H., 2006. “An Autonomous, Underactuated Exoskeleton for Load-carrying Augmentation”. In 2006 IEEE/RSJ International Conference on Intelligent Robots and Systems, IEEE, pp. 1410–1415.
- [8] Kawamoto, H., and Sankai, Y., 2002. “Power assist system HAL-3 for gait disorder person”. In International Conference on Computers for Handicapped Persons, Springer, pp. 196–203.
- [9] Robson, N., and Soh, G. S., 2016. “Geometric design of eight-bar wearable devices based on limb physiological contact task”. *Mechanism and Machine Theory*, **100**, pp. 358–367.
- [10] Sonawale, K. H., Arredondo, A., and McCarthy, J. M., 2013. “Computer aided design of useful spherical Watt I six-bar linkages”. In ASME 2013 International Design Engineering Technical Conferences and Computers and Information in Engineering Conference, American Society of Mechanical Engineers, pp. V06AT07A064–V06AT07A064.
- [11] Wu, J., Purwar, A., and Ge, Q., 2010. “Interactive dimensional synthesis and motion design of planar 6R single-loop closed chains via constraint manifold modification”. *Journal of Mechanisms and Robotics*, **2**(3), p. 031012.
- [12] Soh, G. S., 2014. “Rigid Body Guidance of Human Gait as Constrained TRS Serial Chain”. In ASME 2014 International Design Engineering Technical Conferences and Computers and Information in Engineering Conference, American Society of Mechanical Engineers, pp. V05AT08A063–V05AT08A063.
- [13] Plecnik, M. M., and McCarthy, J. M., 2016. “Computational Design of Stephenson II Six-bar Function Generators for 11 Accuracy Points”. *Journal of Mechanisms and Robotics*, **8**(1), p. 011017.
- [14] Tsuge, B. Y., Plecnik, M. M., and McCarthy, J. M., 2016. “Homotopy Directed Optimization to Design a Six-bar Linkage for a Lower Limb with a Natural Ankle Trajectory”. *Journal of Mechanisms and Robotics*, **8**(6), p. 061009.
- [15] Nymark, J. R., Balmer, S. J., Melis, E. H., Lemaire, E. D., and Millar, S., 2005. “Electromyographic and kinematic nondisabled gait differences at extremely slow overground and treadmill walking speeds”. *Journal of rehabilitation research and development*, **42**(4), p. 523.
- [16] Okita, Y., Tatematsu, N., Nagai, K., Nakayama, T., Nakamata, T., Okamoto, T., Toguchida, J., Ichihashi, N., Matsuda, S., and Tsuboyama, T., 2014. “The effect of walking speed on gait kinematics and kinetics after endoprosthetic knee replacement following bone tumor resection”. *Gait & posture*, **40**(4), pp. 622–627.
- [17] Behrman, A. L., and Harkema, S. J., 2000. “Locomotor training after human spinal cord injury: A series of case studies”. *Physical therapy*, **80**(7), pp. 688–700.
- [18] Sullivan, K. J., Knowlton, B. J., and Dobkin, B. H., 2002. “Step training with body weight support: Effect of treadmill speed and practice paradigms on poststroke locomotor recovery”. *Archives of physical medicine and rehabilitation*, **83**(5), pp. 683–691.
- [19] Plecnik, M. M., and McCarthy, J. M., 2016. “Controlling the movement of a TRR spatial chain with coupled six-bar function generators for biomimetic motion”. *Journal of Mechanisms and Robotics*, **8**(5), p. 051005.
- [20] Plecnik, M., and McCarthy, J., 2015. “Synthesis of an inverted Stephenson linkage to guide a point path”. In The 14th IFToMM World Congress, Taipei, Taiwan, 7 pages, 25-30 October 2015.
- [21] Plecnik, M. M., and McCarthy, J. M., 2016. “Design of Stephenson linkages that guide a point along a specified trajectory”. *Mechanism and Machine Theory*, **96**, pp. 38–51.